Optical Materials 35 (2013) 1571–1576

Contents lists available at SciVerse ScienceDirect

Optical Materials

journal homepage: www.elsevier.com/locate/optmat

Ternary mixed crystal effects on interface optical phonon and electron-interface optical phonon coupling in wurtzite GaN/$Al_xGa_{1-x}N$ quantum wells

Wen-Deng Huang [a,b,*], Guang-De Chen [a], Hong-Gang Ye [a], Ya-Jie Ren [b]

[a] MOE Key Laboratory for Nonequilibrium Synthesis and Modulation of Condensed Matter and Department of Applied Physics, Science of School, Xi'an Jiaotong University, Xi'an 710049, China

[b] School of Physics and Telecommunication Engineering, Shaanxi University of Technology, Hanzhong 723001, China

ARTICLE INFO

Article history:
Received 5 January 2013
Received in revised form 27 February 2013
Accepted 29 March 2013
Available online 22 April 2013

Keywords:
Quantum well
Phonon
Electron–phonon interaction

ABSTRACT

Within the framework of the modified random-element isodisplacement model and dielectric continuum model, the interface optical phonon and electron-interface optical coupling in GaN/$Al_xGa_{1-x}N$ quantum wells with different aluminum concentration are studied in a fully numerical manner. The results show that aluminum concentration has important influence in the interface optical phonon and electron–phonon coupling in GaN/$Al_xGa_{1-x}N$ quantum wells. When the aluminum concentration is lower ($0.03 < x < 0.13$), there are two branches interface optical phonon in high frequency range. When the aluminum concentration is higher ($0.13 < x < 1.00$), there are four branches interface optical phonons in high and low frequency range. Comparing the electron–phonon coupling in lower and higher aluminum concentration range, we found that the electron–phonon coupling in higher aluminum concentration range is stronger.

1. Introduction

Recently, group-III nitrides and their alloys have attracted significant attention due to potential applications in optical, optoelectronic and electronic devices. The properties of alloys may vary over a wide range by changing the composition of alloys [1], which may also offer flexible choices for heterostructures and quantum wells (QWs) with matched lattice constants and expected band gaps covered from red to deep ultraviolet [2]. It is well known that the optical phonons and carrier-phonon interactions play an essential role in many physical processes, such as transport or electron relaxation processed in heterostructures and quantum wells (QWs) [3]. In these confined system, phonon modes are more complicated than those in bulk materials. The electron–phonon interactions are also different from the case of bulk material. Therefore, it is of interest to investigate the polar optical phonons and electron–phonon interaction in wurtzite heterostructures and quantum wells (QWs).

Due to anisotropy of wurtzite crystal, it has been found that the interface optical phonons, propagating optical phonons, confined optical phonons, half optical phonon and exactly confined optical phonons may coexist in wurtzite heterostructures and QWs [4,5]. Within the framework of the dielectric-continuum (DC) model [6,7] and modified dielectric-continuum (MDC) model [8,9] based on the well known Born–Huang equation [10], the interface optical phonons and electron–phonon interaction in wurtzite heterostructures were studied in Refs. [11–13]. The propagating optical phonons and electron–phonon interaction were investigated in Refs. [14,15]. The quasi-confined optical phonons and their electron–phonon interaction were also researched in Refs. [16,17]. However, to the best of our knowledge, most of the work published so far focused on optical phonons in heterostructures/quantum wells (QWs) composed of binary wurtzite crystal, the optical phonons in wurtzite quantum wells/heterostructures consisted of mixed crystal have not been investigate in detail. More recently Qu and Ban have researched ternary mixed crystal effect on electron mobility in a strained wurtzite AlN/GaN/AlN quantum well with an $In_xGa_{1-x}N$ nanogroove, and do not discuss the mixed crystal effects on optical phonons [18]. In this paper, we only consider the interface optical (IO) phonons, electron–phonon coupling and ternary mixed crystal effect on interface optical phonons in wurtzite GaN/$Al_xGa_{1-x}N$ quantum wells.

The paper is organized in the following way. In Section 2, we present a general theoretic description of the model and necessary formula. In Section 3, the numerical results for interface optical (IO) phonons, electron–phonon coupling and ternary mixed crystal effect on interface optical phonons in GaN/$Al_xGa_{1-x}N$ QWs are

* Corresponding author at: MOE Key Laboratory for Nonequilibrium Synthesis and Modulation of Condensed Matter and Department of Applied Physics, Science of School, Xi'an Jiaotong University, Xi'an 710049, China. Tel.: +86 02982663128.
E-mail address: wdhuang2005@163.com (W.-D. Huang).

0925-3467/$ - see front matter © 2013 Elsevier B.V. All rights reserved.
http://dx.doi.org/10.1016/j.optmat.2013.03.032

given and discussed. Finally, we present the main results and conclusions of this work in Section 4.

2. Theory

2.1. The optical phonons in wurtzite crystals

Group-III nitrides usually crystallize in the hexagonal wurtzite structure, the primitive cell contains four atoms. There are ordinary and extraordinary optical phonons in wurtzite crystals due to the anisotropy of crystal [4,5]. The ordinary phonons are always transverse and polarized in the *xy*-plane with $E_1(x, y)$ symmetry, and decoupled from other vibration modes. We will not discuss them here. The extraordinary phonons are associated with *z*- and *x*–*y* polarized vibrations, the *z*-polarized mode has $A_1(z)$ symmetry, while the *xy*-polarized one has $E_1(x, y)$ symmetry. The A_1 and E_1 modes are split into longitudinal optical (LO) and transverse-optical (TO) component. The dispersion relation of the extraordinary phonons in wurtzite crystal is described by [19]

$$\varepsilon_\perp(\omega)q_\perp^2 + \varepsilon_z(\omega)q_z^2 = 0 \tag{1}$$

with

$$\varepsilon_\perp(\omega) = \varepsilon_\perp^{(\infty)}\frac{\omega^2-\omega_{\perp,L}^2}{\omega^2-\omega_{\perp,T}^2}, \quad \varepsilon_z(\omega) = \varepsilon_z^{(\infty)}\frac{\omega^2-\omega_{z,L}^2}{\omega^2-\omega_{z,T}^2} \tag{2}$$

where $\varepsilon_\perp(\omega)$ and $\varepsilon_z(\omega)$ are the dielectric constants in perpendicular direction and the parallel direction of the *z* axis. $\omega_{\perp,L}$, $\omega_{z,L}$, $\omega_{\perp,T}$, and $\omega_{z,T}$ are the zone center E_1(LO), A_1(LO), E_1(TO) and A_1(TO) phonon frequencies of the bulk materials, respectively.

The frequencies of A_1(LO), A_1(TO), E_1(LO) and E_1(TO) optical phonons in wurtzite ternary mixed crystals $A_xB_{1-x}C$ depend on the concentration of A or B. Considering only nearest–neighbor interaction, using the modified random-element isodisplacement model [20] and uniaxial model [21], the phonon governing equation for wurtzite ternary mixed crystal $A_xB_{1-x}C$ in long wavelength limit are given as follows:

$$m_A\ddot{\vec{u}}_{Ai} = -F_{ai}(\vec{u}_{Ai}-\vec{u}_{Ci}) - e_{ai}\vec{E}_{loc,i} \tag{3}$$

$$m_B\ddot{\vec{u}}_{Bi} = -F_{bi}(\vec{u}_{Bi}-\vec{u}_{Ci}) - e_{bi}\vec{E}_{loc,i}, \tag{4}$$

$$m_C\ddot{\vec{u}}_{Ci} = -(1-x)F_{bi}(\vec{u}_{Ci}-\vec{u}_{Bi}) - xF_{ci}(\vec{u}_{Ci}-\vec{u}_{Ai}) + \{(1-x)e_{bi} + xe_{ci}\}\vec{E}_{loc,i} \tag{5}$$

$$E_{loc,i} = E_i + \frac{4\pi}{3}\gamma_i P_i \tag{6}$$

$$P_i = x\left\{\frac{e_{ai}}{v_a}(\vec{u}_{Ci}-\vec{u}_{Ai}) + \frac{\alpha_{Ci}+\alpha_{Ai}}{v_b}E_{loc,i}\right\}\frac{v_a}{v} + (1-x)\left\{\frac{e_{bi}}{v_b}(\vec{u}_{Ci}-\vec{u}_{Bi}) + \frac{\alpha_{Ci}+\alpha_{Bi}}{v_b}E_{loc,i}\right\}\frac{v_b}{v} \tag{7}$$

Where the subscript *i* stand for *z*- and ⊥(*x*–*y* plane) polarization directions, the other subscripts *a* and *b* refer to binary materials *AC* and *BC*, respectively. Here, *m* and u_i are the mass and *i*th component of displacement of the ions *A*, *B*, and *C*. F_{ai} and F_{bi} are effective nearest-neighbor force constants, *v* is the volume of the unitcell of the mixed crystal while v_a and v_b are the unit cellvolumes of the binary materials *AC* and *BC*, respectively. The dielectric function ε_i of the ternary semiconductor is defined by the usual expression between the macroscopic field E_i and the polarization P_i, i.e., $P_i = (\varepsilon_i-1)E_i/4\pi$. The local field $E_{loc,i}$ deviates from the Lorentz relation, which is expressed by introducing γ_i, we take $\gamma_z = 1 - 0.1\times(3/4\pi)$ and $\gamma_\perp = 1 + 0.2\times(3/4\pi)$ [20]. The frequencies of A_1(LO), A_1(TO), E_1(LO) and E_1(TO) optical phonons in wurtzite ternary mixed crystals $A_xB_{1-x}C$ are obtained from Eqs. (3)–(7) as the following:

$$\omega_{Xi}^2 = \frac{\Omega_{Xbi}^2+\Omega_{Xai}^2}{2} \pm \left[\left(\frac{\Omega_{Xbi}^2-\Omega_{Xai}^2}{2}\right)^2 + x(1-x)\Omega_{Xbai}^4\right]^{1/2} \tag{8}$$

$$\Omega_{Xbi}^2 = \omega_{bi}^2 + (1-x)\alpha_{Xi}\omega_{bi'}^2 \tag{9}$$

$$\Omega_{Xai}^2 = \omega_{ai}^2 + x_{Xi}\omega_{ai'}^2 \tag{10}$$

$$\Omega_{Xbai}^4 = \left[\left(\frac{\delta_{bi}}{\delta_{ai}}\right)^{1/2}\beta_{Xi}\omega_{bi'}\omega_{ai'} + \frac{\overline{\mu}}{m_C}\omega_{Ai}^2\right] \times \left[\left(\frac{\delta_{ai}}{\delta_{bi}}\right)^{1/2}\beta_{Xi}\omega_{bi'}\omega_{ai'} + \frac{\overline{\mu}}{m_C}\omega_{Bi}^2\right] \tag{11}$$

$$\beta_{Ti} = -\gamma_i, \beta_{Li} = (3-\gamma_i)/\varepsilon_{\infty i} \tag{12}$$

$$\overline{\mu} = \sqrt{\mu_a\mu_b} \tag{13}$$

where *X* stands for longitudinal LO and TO components. $\mu_a(\mu_b)$ is the reduced mass of binary crystal AC (BC), The high-frequency dielectric constant in ternary $A_xB_{1-x}C$ is

$$\frac{\varepsilon_{\infty i}-1}{3+\gamma_i(\varepsilon_{\infty i}-1)} = x\frac{v_a}{v}\frac{\varepsilon_{\infty ai}-1}{3+\gamma_i(\varepsilon_{\infty ai}-1)} + (1-x) \times \frac{\varepsilon_{\infty bi}-1}{3+\gamma_i(\varepsilon_{\infty bi}-1)} \tag{14}$$

The other quantities are given by

$$\omega_{ai}^2 = \omega_{ai}^2\left(1-(1-x)\frac{u_a}{m_C}\right) \tag{15}$$

$$\omega_{ai}'^2 = \left[\delta_{ai}\frac{v_a}{v}\frac{3+\gamma_i(\varepsilon_{\infty i}-1)}{\gamma_i(3+\gamma_i(\varepsilon_{\infty ai}-1)}\left(\omega_{Ai}^2-\omega_{Tai}^2\right)\right] \tag{16}$$

$$\omega_{Ai}^2 = \frac{3+(\varepsilon_{\infty ai}-1)}{3+\gamma_i(\varepsilon_{\infty ai}-1)}\omega_{Tai}^2 \tag{17}$$

$$\delta_{ai} = 1 - x\frac{u_a}{m_C}\left(1-\frac{e_{bi}}{e_{ai}}\right) \tag{18}$$

By interchanging *a* by *b* and *x* by 1−*x*, we can obtained the other variables ω_{bi}, ω_{bi}', ω_{Ai} and δ_{bi}

2.2. The interface optical phonon and electron-interface phonon interaction in wurtzite quantum wells

We consider an arbitrary wurtzite symmetry multilayer heterostructures grown along the optical axis *c* of crystal. The interfaces are located at $z = z_j$ ($j = 0, 1, \ldots, n-1, n$). We take the *z* axis along the direction of the *c* axis (see (a) in Fig. 1). With the framework of DC model, the potential of polar optical phonons in the layer *j* satisfies the Poisson equation in the absence of free charge,

$$\varepsilon\nabla^2\varphi(r) = \left\{\varepsilon_\perp(\omega)\left[\frac{\partial^2}{\partial x^2}+\frac{\partial^2}{\partial y^2}\right] + \varepsilon_z(\omega)\frac{\partial^2}{\partial z^2}\right\}\psi(r) = 0 \tag{19}$$

For the quasi-two-dimensional confined structure, the potential of optical phonons is given by

$$\psi(r) = \sum_{q_\perp} e^{iq_\perp\cdot\rho}\varphi(z) \tag{20}$$

where $q_\perp$ and ρ are the two-dimensional wave vector and position vector in *x*–*y* plane. Substituting Eq. (1) and (20) into (19), we finally get

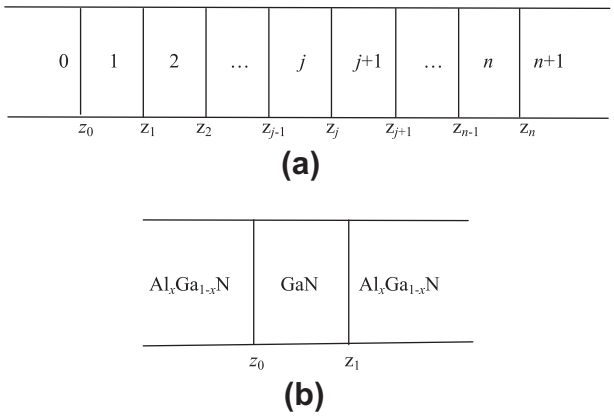

Fig. 1. (a) A general multilayer wurtizte Q2D heterostructures. (b) A single GaN/$Al_xGa_{1-x}N$ QW.

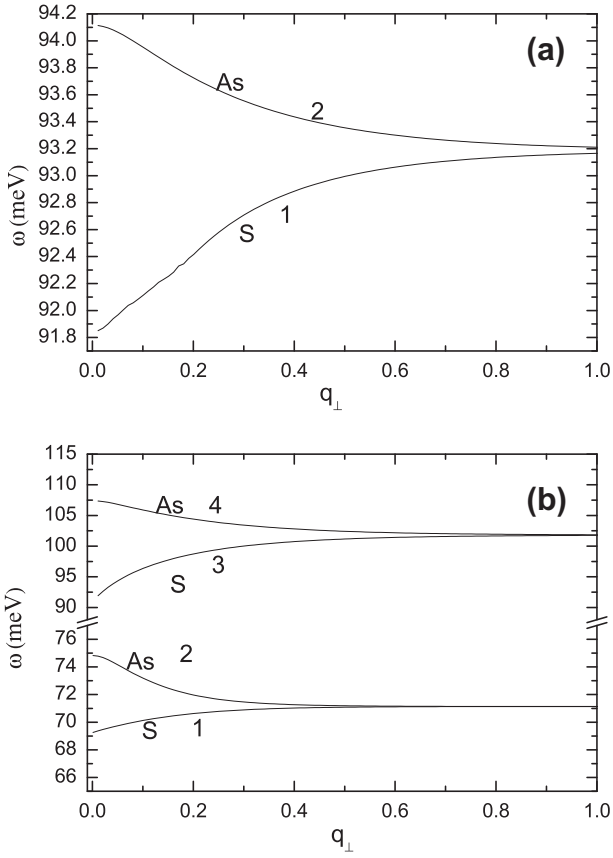

Fig. 2. Dispersion curves of IO phonon modes for a GaN QW of width $d = 5$ nm sandwiched between two semi-infinite $Al_xGa_{1-x}N$ barrier lays. Here (a) for $x = 0.10$ and (b) for $x = 0.80$.

$$\left[\varepsilon_z(\omega)\frac{\partial^2}{\partial z^2} - q_\perp^2\varepsilon_\perp(\omega)\right]\varphi(z) = 0 \text{ or } \frac{\partial^2\varphi(z)}{\partial z^2} + q_z^2\varphi(z) = 0. \tag{21}$$

The solutions of Eq. (21) should satisfy the following electrostatic boundary conditions at $z = z_j$, namely

$$\varphi_j(z)\Big|_{z=z_j} = \varphi_{j+1}(z)\Big|_{z=z_j} \tag{22}$$

$$\varepsilon_{j,z}(\omega)\frac{\partial\varphi_j(z)}{\partial z}\Big|_{z=z_j} = \varepsilon_{j+1,z}(\omega)\frac{\partial\varphi_{j+1}(z)}{\partial z}\Big|_{z=z_j} \tag{23}$$

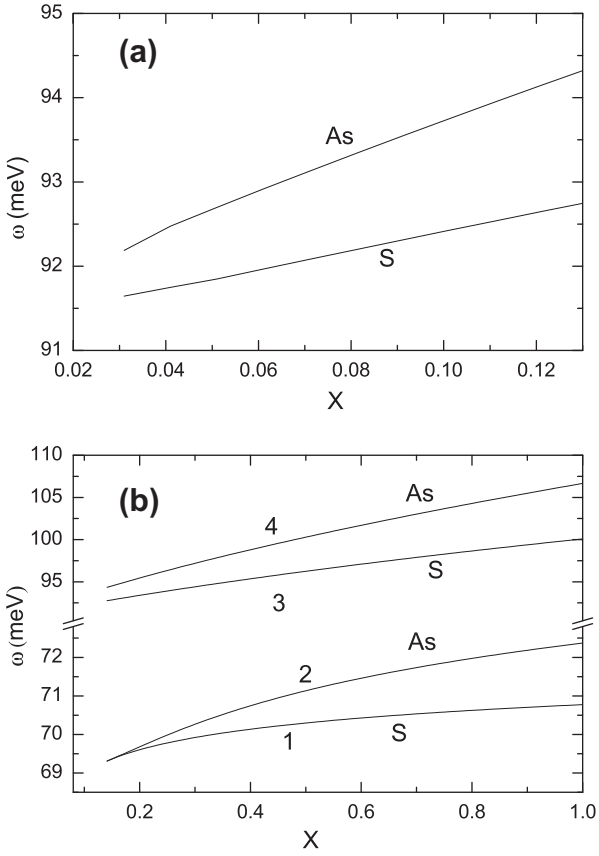

Fig. 3. The effects of aluminum concentration (x) on dispersion curves of IO phonons for the same QW as in Fig. 2 ($q_\perp = 0.20$). Here (a) for $0.02 < x < 0.13$, and (b) for $0.13 < x < 1.00$.

$$\varphi_j(z)\Big|_{z\to\pm\infty} = 0 \tag{24}$$

For the structure we study here, the potential of optical phonon can be obtained from Eqs. (20) and (21) as following:

$$\psi_j(r) = \sum_{q_\perp} e^{iq_\perp\cdot\rho}\left[A_j e^{iq_{zj}(z-z_j)} + B_j e^{-iq_{zj}(z-z_j)}\right] \tag{25}$$

For interface optical phonon modes, $\varepsilon_\perp(\omega)\varepsilon_z(\omega) > 0$, and $q_{z,j}$ is an imaginary in layer j [4,5]. Using the boundary conditions (22)–(24) at the $z = z_j$ interface successively, the dispersion relation of IO phonons in an arbitrary multilayer system can be obtained [22,23]. For a single wurtzite symmetry quantum wells, we can obtain the dispersion relation as following

$$2q_{z,0}\varepsilon_{z,0}q_{z,1}\varepsilon_{z,1} + \frac{q_{z,0}^2\varepsilon_{z,0}^2 + q_{z,1}^2\varepsilon_{z,1}^2}{q_{z,0}\varepsilon_{z,0}q_{z,1}\varepsilon_{z,1}}\tanh(q_{z,1}d_1) = 0 \tag{26}$$

In Eq. (26), we use index 1 for quantum well material and 0 for the barrier material, d_1 is the width of the quantum well. Generally, From Eq. (26), we can obtain the same relation in Ref. [24]. Eq. (26) has a definite number solutions with definite symmetry with respect to symmetric center of the QW structure for a given phonon wave vector $q_\perp$ (see Figs. 4 and 5). Our numerical calculations show that the IO phonons exist in different frequency range with different concentration of aluminum (x) in GaN/$Al_xGa_{1-x}N$ QWs.

By using a standard quantization procedure [25–27], the electron–phonon interaction Hamiltonian for the IO phonon modes in wurtzite multilayer heterostructures can be obtained as follows:

$$H_{e-ph} = \sum_m\sum_{q_\perp} e^{i\vec{q}_\perp\cdot\vec{\rho}}\,\Gamma_m(q_\perp, z)\left[\hat{\alpha}_m(\vec{q}_\perp) + \hat{\alpha}_m^+(-\vec{q}_\perp)\right]. \tag{27}$$

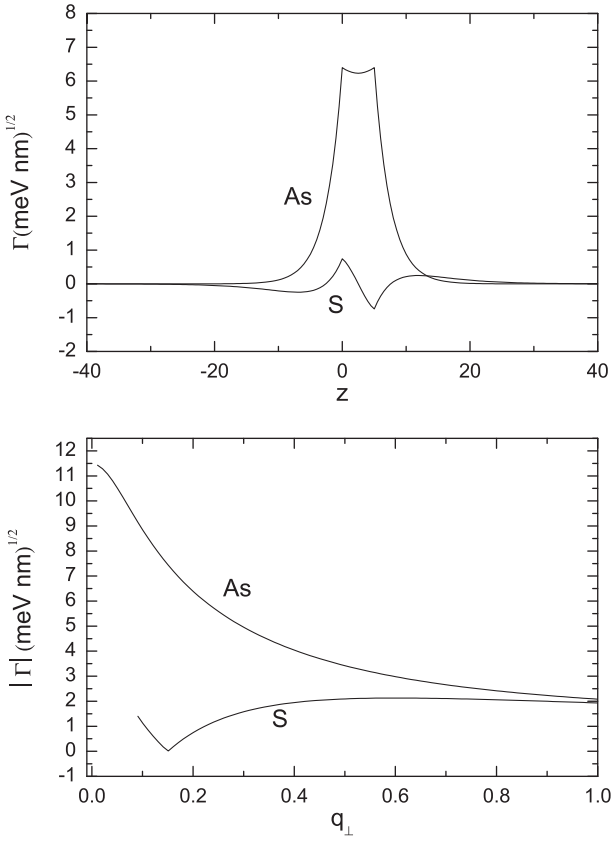

Fig. 4. Electron-IO phonon coupling functions $\Gamma_m(q_\perp, z)$ in the same QW as in Fig. 2 with aluminum concentration $x = 0.10$. (a) The Spatial dependence of the electron-IO phonon coupling functions $\Gamma_m(q_\perp, z)$ with the wave number $q_\perp = 0.20$ (b) The wave-vector dependence of the electron-IO phonon coupling functions $\Gamma_m(q_\perp, z)$ with z = nm.

where $\Gamma_m(q_\perp, z)$ is electron–phonon coupling functions, which describe the coupling strength of single electron at the position z with the mth IO phonon modes, and is given by

$$\Gamma_m(q_\perp, z) = B_0\left(\frac{\hbar e^2}{8A\varepsilon_0\omega_m(q_\perp)}\right)^{\frac{1}{2}}\begin{cases} f_1(q_\perp, z), z < z_0, \\ f_2(q_\perp, z), z_{j-1} < z < z_j, j = 1, 2, 3\cdots\cdots n-1 \\ f_3(q_\perp, z), z > z_n, \end{cases} \tag{28}$$

where A is the cross-sectional area of the heterostructures, B_0 can obtained from the orthogonal relation [3,12]. The normal frequency $\omega_m(q_\perp, z)$ of the mth branch of the IO phonon modes can be obtained by solving the dispersion relation Eq. (26). For a single wurtzite symmetry quantum wells, f_i $(q_\perp, z)$ $(i = 1, 2, 3)$ are given out as following,

$$\begin{aligned} f_1(q_\perp, z) = {} & \alpha_{-,0}e^{q_\perp(z-z_0)} + (\alpha_{+,0} - \alpha_{-,0})e^{q_{z,0}(z-z_0)} + A_2a_{+,2}e^{q_\perp(z-z_1)} \\ & + (B_1a_{-,1} - A_1a_{+,1})e^{q_\perp(z-z_1)} + (A_1a_{+,1}e^{q_{z,1}d_1} \\ & - B_1a_{-,1}e^{-q_{z,1}d_1})e^{q_\perp(z-z_0)} \end{aligned} \tag{29}$$

$$\begin{aligned} f_2(q_\perp, z) = {} & \alpha_{+,0}e^{q_\perp(z-z_0)} + (A_1e^{-q_{z,1}(z-z_1)} + B_1e^{q_{z,1}(z-z_1)})(a_{+,1} \\ & - a_{-,1}) + (A_1a_{-,1}e^{q_{z,1}d_1} - B_1a_{+,1}e^{-q_{z,1}d_1})e^{-q_\perp(z-z_0)} \\ & + (B_1a_{-,1} - A_1a_{+,1})e^{q_\perp(z-z_1)} + A_2a_{+,2}e^{q_\perp(z-z_1)} \end{aligned} \tag{30}$$

$$\begin{aligned} f_3(q_\perp, z) = {} & \alpha_{+,0}e^{q_\perp(z-z_0)} \\ & + \left[(B_1a_{+,1} - A_1a_{-,1})e^{q_\perp d_1} + A_1a_{-,1}e^{q_{z,1}d_1} - B_1a_{+,1}e^{-q_{z,1}d_1}\right]e^{q_\perp(z-z_0)} \\ & + A_2\left[e^{q_{z,2}(z_1-z)}(a_{+,2} - 1) + a_{-,2}e^{-q_\perp(z-z_1)}\right] \end{aligned} \tag{31}$$

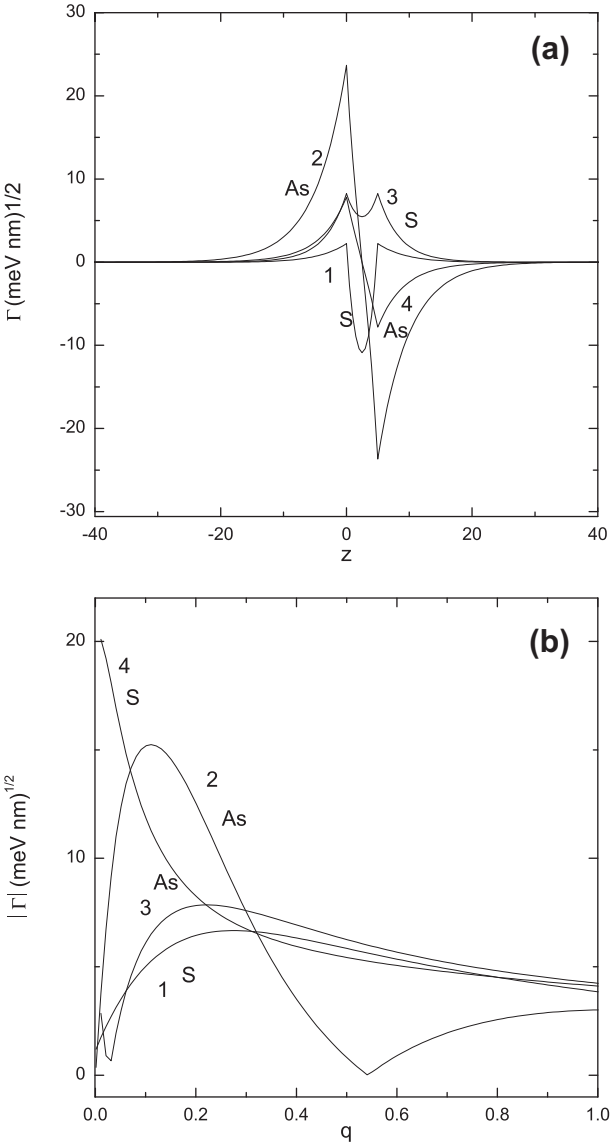

Fig. 5. Same as in Fig. 4, but for $x = 0.80$.

In Eqs. (17)–(19), A_j, B_j can be obtained by using boundary conditions [12]. $\alpha_{\pm,j}$ is defined as the following:

$$a_{\pm,j} = \frac{1 \pm \gamma_j}{q_{z,j} \pm q_\perp} \tag{32}$$

3. Numerical results and discussion

In order to further study the interface optical (IO) phonons, electron–phonon coupling and ternary mixed crystal effect on interface optical phonons in wurtzite heterostructures/QWs. Numerical calculations on GaN/Al_xGa_{1-x}N single QW (see (b) in Fig. 1) have been performed. The corresponding physical parameters [12,28,29] are listed in Table 1.

In order to see the behavior of interface optical phonons with different aluminum concentration, we plot the dispersions of IO phonons in GaN/Al_xGa_{1-x}N symmetry single QW in Fig. 2. Our calculations indicate that the interface optical phonons appear in two aluminum concentration range, namely the aluminum concentration range (0.03, 0.13) and (0.13, 1.00). If the aluminum concentration x is in the interval (0.03, 0.13), there are two IO phonon

Table 1
Optical phonon energies (in meV), dielectric constants, effective charge (in e_0) and other parameters in calculations.

Material	$\omega_{z,T}$	$\omega_{\perp,T}$	$\omega_{z,L}$	$\omega_{\perp,L}$	$\varepsilon_{\infty,z}$	$\varepsilon_{\perp,z}$	e_z	$e_\perp$	a	c
GaNAlN	65.91[a]	69.25[a]	90.97[a]	91.83[a]	6.38[b]	6.11[b]	2.86[b]	2.69[b]	3.20[b]	5.22[b]
	75.72[c]	83.13[c]	110.13[c]	113.02[b]	5.36[b]	5.17[b]	2.85[b]	2.70[b]	3.10[b]	5.01[b]

[a] Ref. [13].
[b] Ref. [30].
[c] Ref. [29].

branches in high frequency range ($\omega_{\perp,L1}$, $\omega_{\perp,L0}$), and no IO phonon branches in low frequency range ($\omega_{\perp,T1}$, $\omega_{\perp,T0}$). When the aluminum concentration x is in the interval (0.13, 1.00), there exist four IO phonon branches in two frequency ranges (labeled 1, 2, 3, and 4 from lower to higher frequency). When the aluminum concentration x is in the range (0.00, 0.03), there are no IO phonons. In the Refs. [12,13,30], the authors think that the IO phonons exist in high frequency range and low frequency range, the branches of IO phonons is 4. Our numerical results clearly indicate that this is not true. The aluminum concentration x affect the behavior of IO phonons in GaN/Al_xGa_{1-x}N QWs greatly. Furthermore, numerical calculation also show that the frequencies of interface optical phonons in low frequency range approach a common limit with the increase of $q_\perp$, another common limit can be reached for the high frequency range. The common limit in each frequency range is different with different aluminum concentration.

We also plotted the relation between the IO phonon frequencies and aluminum concentration (x) in Fig. 3. The results shows that the IO phonon frequencies in high frequency range increase almost linearly with increasing aluminum concentration (0.03, 1.00), which characterized by linearity. The IO phonon frequencies in low frequency range, which do not increase almost linearly with low aluminum concentration changes (0.13, 0.60). With the increase of the aluminum concentration in the range (0.60, 1.00), the IO frequencies in low frequency range appear linear increase. So the empirical formula in Ref. [31] can not been used to investigate all physical properties in quantum wells composed of wurtzite mixed crystal. The mixed crystal effects will change the properties greatly, and will appear in many optical and electronic experiments which related to the phonon modes. The IO phonons play important role in Raman spectra. In recent years, many investigations have been carried out by Raman scattering experiment, the IO phonons were also observed [32,33]. We believe that our numerical results will be helpful for further investigations of optical properties in wurtzite quasi-two-dimensional (Q2D) quantum heterostructures.

In Figs. 4 and 5, the electron-IO phonon coupling functions $\Gamma_m(q_\perp, z)$ in single GaN/Al_xGa_{1-x}N QW with different aluminum concentration are plotted (x = 0.10, 0.80). The calculations clearly show that electron-IO phonon coupling functions have exactly symmetry with respect to the center of the QW structure. If the aluminum concentration x is in the range (0.03, 0.13) (please see the Fig. 4), the electron-IO phonon coupling function for the anti-symmetric modes are greater than that for the symmetric modes. The electron-IO phonon couplings decrease to 0 when z goes to infinity. The electron-IO phonon interactions are mainly located in quantum well, and have maximum at interface. From Fig. 4, we can also see that the long-wavelength optical phonons are more important for electron–phonon interaction than short wavelength optical phonons. The electron-IO phonon coupling function for anti-symmetric modes are more important than symmetric modes. If aluminum concentration x is in the range (0.13, 1.00), (please see the Fig. 5), the modes 1 and 3 (2 and 4) (labeled from lower to higher frequency) are exactly symmetric (anti-symmetric) modes. The modes 2 and 4 have more important effect on electron–phonon interaction when the wave number $q_\perp$ is smaller than 0.28. When $q_\perp$ is greater than 0.28, the modes 1, 3 and 4 have more important effects on electron–phonon interaction. Comparing Fig. 4 with Fig. 5, we can draw a conclusion that the electron-IO phonon couplings with higher aluminum concentration are more important. Our numerical results indicate that the behavior of electron-IO phonon in GaN/Al_xGa_{1-x}N QWs is very different from that in QWs composed of binary crystal [12–15]. The ternary mixed crystal effects influence the electron-IO phonon interactions, which also observed by Raman Spectroscopy experiments [33].

In order to see the effect of ternary mixed crystals on electron-IO phonon interaction, the electron-IO phonon coupling function $|\Gamma_m(q_\perp, z)|$ versus the aluminum concentration (x) are also plotted in Fig. 6. If aluminum concentration x is changed in the range (0.03, 0.13), we can observe that the electron–phonon interactions in high frequency range almost increase linearly with increase of aluminum concentration, which characterized by linearity. If aluminum concentration x is increased in the range (0.13, 1.00), we can see that the electron–phonon couplings (modes 3 and 4) in high frequency range also character-

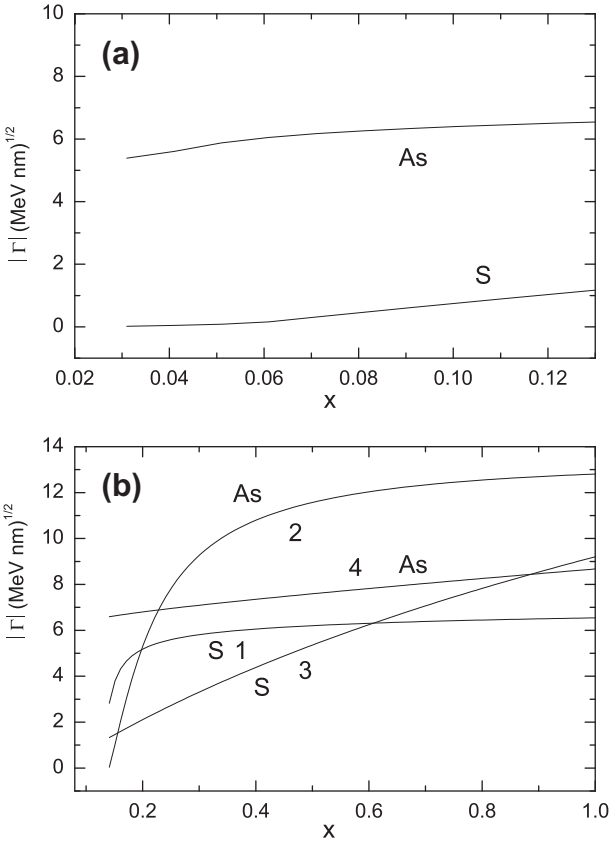

Fig. 6. The effect of aluminum concentration (x) on electron–phonon coupling functions $\Gamma_m(q_\perp, z)$ for the IO phonons in the same QW as in Fig. 1 ($q_\perp$ = 0.20). Here (a) for 0.02 < x < 0.13 and (b) for 0.13 < x < 1.00.

ized by linear increase. For the IO phonons in low frequency range (modes 1 and 2), their electron–phonon couplings indicate nonlinear changes with increasing aluminum concentration (x). From these figures, we also observe that the electron-IO phonon couplings with higher aluminum concentration are more important.

4. Conclusion

In conclusion, we have investigated the IO phonons and electron–phonon interaction in wurtzite GaN/$Al_xGa_{1-x}N$ QWs with different aluminum concentration by using the modified random-element isodisplacement model and DC model. We found that the ternary mixed crystal effects influence the IO phonon and electron-IO phonon interactions greatly. When the aluminum concentration (x) is in the range (0.03, 0.13), only two branches appear in high frequency range. When x is in the range (0.13, 1.00), the four branches of IO phonon appear in high frequency range and low frequency range. The IO phonon frequencies and electron-IO phonon coupling in high frequency range increase almost linearly with increasing aluminum concentration. But for the IO phonons in low frequency range, which do not increase almost linearly with concentration changes. The electron-IO phonon interactions in higher aluminum concentration (x) and low frequency range are more important. We hope these results and conclusion would be helpful for the further experimental and theoretical investigations of optical properties in wurtzite Q2D heterostructures.

Acknowledgements

This work was supported by the National Natural Science Foundation of China (Grant Nos. 11074200 and 51106093), Scientific Research Program Funded by Shaanxi Provincial Education Department, Shaanxi Province, China (Grant No. 12JK0982)

References

[1] S. Nakamura, G. Fasol, The Blue Laser Diodes: GaN Light Emitters and Lasers, Springer, Berlin, 1997.
[2] H. Hirayama, A. Kinoshita, T. Yamabi, Y. enomoto, A. Hirata, T. Araki, Y. Nanishi, Y. Aoyagi, Appl. Phys. Lett. 80 (2002) 207.
[3] M.A. Stroscio, M. Dutta, Phonons in Nanostructures, Cambridge University Press, Cambridge, 2001.
[4] S.M. Komirenko, K.W. Kim, M.A. Stroscio, Phys. Rev. B 59 (1999) 5013.
[5] B.C. Lee, K.W. Kim, M.A. Stroscio, M. Dutta, Phys. Rev. B58 (1998) 4860.
[6] R. Fuchs, K.L. Kliewer, Phys. Rev. 140 (1965) A2076.
[7] J. Licari, R. Evrard, Phys. Rev. B 15 (1977) 2254.
[8] K. Huang, B.F. Zhu, Phys. Rev. B 38 (1988) 13377.
[9] R. Haupt, L. Wendler, Phys. Rev. B 44 (1991) 1850.
[10] M. Born, K. Huang, Dynamical Theory of Crystal Lattices, Clarendon Press, Oxford, 1954.
[11] L. Zhang, J.J. Shi, T.L. Tansley, Phys. Rev. B 71 (2005) 245324.
[12] J.J. Shi, Phys. Rev. B 68 (2003) 165335.
[13] Y. Yang, C. Cheng, Opt. Mater. 34 (2012) 832.
[14] J.J. Shi, X.L. Chu, Phys. Rev. B 70 (2004) 115318.
[15] W.D. Huang, Y.J. Ren, Eur. Phys. J. Appl. Phys. 57 (2012) 11301.
[16] J.T. Lü, J.C. Cao, Phys. Rev. B 71 (2005) 155304.
[17] W.D. Huang, S.Y. Wei, J. Lumin. 126 (2007) 413.
[18] Y. Qu, S.L. Ban, J. Appl. Phys. 110 (2011) 013722.
[19] R. Loudon, Adv. Phys. 13 (1964) 423.
[20] S. Yu, K.W. Kim, L. Bergman, M. Dutta, M.A. Stroscio, J.M. Zavada, Phys. Rev. B 58 (1998) 15283.
[21] W. Hayes, R. Loudon, Scattering of Light by Crystal, Wiley, New York, 1978.
[22] L. Wendler, R. Haupt, Phys. Stat. Sol. (b) 141 (1987) 493.
[23] S. Yu, K.W. Kim, M.A. Stroscio, G.J. Iafrate, J.P. Sun, G.I. Haddad, J. Appl. Phys. 82 (1997) 3363.
[24] L. Wendler, R. Pechstedt Phys, Stat. Sol. (b) 141 (1987) 129–150.
[25] E.L. Albuquerque, J. Phys. C 13 (1980) 2623.
[26] L. Wendler, Phys. Status Solidi B 129 (1985) 513.
[27] L. Wendler, R. Haupt, Phys. Status Solidi B 143 (1987) 487.
[28] W.D. Huang, G.D. Chen, Y.J. Ren, J. Appl. Phys. 112 (2012) 053704.
[29] C. Burgaro, K. Rapcewicz, J. Bernholc, Phys. Rev. B 61 (2000) 6720.
[30] D. Romanov, V. Mitin, M. Stroscio, Phys. Rev. B 66 (2002) 115321.
[31] D. Behr, R. Niebuhr, J. Wagner, K.H. Bachem, U. Kaufmann, in: C.R. Abernathy, H. Amano, J.C. Zolper (Eds.), Galliun and Related materials II, Materials Research Society, Pittsburgh, 1997.
[32] Dimitri Alexson, Leah Bergman, Robert J. Nemanich, Mitra Dutta, Michael A. Stroscio, C.A. Parker, S.M. Bedair, N.A. El-Masry, Fran Adar, J. Appl. Phys. Lett. 89 (2000) 798.
[33] M. Dutta, D. Alexson, L. Bergman, Physical E 11 (2001) 277.